proteomicsNOW.com

# Save the date October 17

Join thought leaders at the **ProteomicsNOW Virtual Conference** to find out about the latest advances in mass spectrometry in proteomics. Share best practices and explore new technologies and techniques that can help improve your research results.

**Over 12 hours of**

- Live webinars
- Lightning rounds
- Poster sessions
- Panel discussions

## Speakers' spotlight

**Kathryn Lilley**
University of Cambridge

**Noah Dephoure**
Weill Cornell Medical College

**Lan Huang**
University of California, Irvine

**Roman Fischer**
University of Oxford

**Sina Ghaemmaghami**
University of Rochester

To find out more and view a full list of speakers, please visit **proteomicsnow.com**

Co-sponsored by:
ThermoFisher SCIENTIFIC

WILEY

THE PROTEIN SOCIETY

# METHODS AND APPLICATIONS

# Weak IgG self- and hetero-association characterized by fluorescence analytical ultracentrifugation

**Danlin Yang,[1] John J. Correia,[2] Walter F. Stafford III,[3] Christopher J. Roberts,[4] Sanjaya Singh,[5] David Hayes,[1] Rachel Kroe-Barrett,[1] Andrew Nixon,[1] and Thomas M. Laue[6]***

[1]Biotherapeutics Discovery Research, Boehringer Ingelheim Pharmaceuticals, Inc., Ridgefield, Connecticut 06877
[2]Department of Biochemistry, University of Mississippi Medical Center, Jackson, Mississippi 39216
[3]Department of Systems Biology, Harvard Medical School, Boston, Massachusetts 02115
[4]Department of Chemical and Biomolecular Engineering, University of Delaware, Newark, Delaware 19716
[5]Janssen BioTherapeutics, Janssen Research and Development, LLC, Spring House, Pennsylvania 19477
[6]Department of Molecular, Cellular and Biomedical Sciences, University of New Hampshire, Durham, New Hampshire 03861

Received 15 February 2018; Accepted 2 April 2018
DOI: 10.1002/pro.3422
Published online 10 April 2018 proteinscience.org

**Abstract: Weak protein–protein interactions may be important to binding cooperativity. A panel of seven fluorescently labeled tracer monoclonal IgG antibodies, differing in variable (V) and constant (C) region sequences, were sedimented in increasing concentrations of unlabeled IgGs of identical, similar, and different backgrounds. Weak IgG::IgG attractive interactions were detected and characterized by global analysis of the hydrodynamic nonideality coefficient, $k_s$. The effects of salt concentration and temperature on $k_s$ suggest the interactions are predominantly enthalpic in origin. The interactions were found to be variable in strength, affected by both the variable and constant**

*Abbreviations:* mAb, Monoclonal Antibody; V, Variable; C, Constant; AUC, Analytical Ultracentrifugation; SV, Sedimentation Velocity; FDS, Fluorescence Detection System; IEF, Isoelectric Focusing; CEX, Cation Exchange Chromatography; MCE, Membrane Confined Electrophoresis; AF, Alexa Fluor; UV, Ultraviolet; $k_s$, Hydrodynamic nonideality coefficient; $k_{s,ii}$, Self-term hydrodynamic nonideality coefficient; $k_{s,ij}$, Cross-term hydrodynamic nonideality coefficient; B, Second virial coefficient; f = Frictional coefficient; $f^0$ = Frictional coefficient at infinite dilution; $\gamma$ = Activity coefficient; c = Concentration; s = Sedimentation coefficient; $s_w$ = Weight-average sedimentation coefficient; $s_{20,w}$ = Corrected weight-average sedimentation coefficient at 20°C; $s^*$ = Apparent sedimentation coefficient; $s^0$ = Sedimentation coefficient at infinite dilution; $g(s^*)$ = Apparent sedimentation coefficient distribution function; s(c) = Concentration dependence of sedimentation coefficient; $D^0$ = Diffusion coefficient at infinite dilution; D(c) = Concentration dependence of diffusion coefficient; M = Molecular weight; pI, Isoelectric point; $\bar{U}$, Partial specific volume; $\mu$, Electrophoretic mobility; $Z_{eff}$, Effective charge; $Z_{DHH}$, Debye- Hückel-Henry charge; $k_B$, Boltzmann's constant; $\kappa$, Inverse Debye length; a, Sum of the Stokes radii of the macromolecule and its counterion.

Additional Supporting Information may be found in the online version of this article.

**Word statement**: The significance of the present work on the investigation of weak interactions between IgG molecules has several implications: (1) source of high viscosity in formulation development; (2) self-association in serum/high concentration fluids in vivo; and (3) contribution of cooperative interactions in antibody effector activations.

*Correspondence to: Thomas M. Laue, Department of Molecular, Cellular and Biomedical Sciences, University of New Hampshire, Durham, NH 03861. E-mail: tom.laue@unh.edu

**regions, but indiscriminate with respect to IgG subclass. Furthermore, weak attractive interactions were observed for all the mAbs with freshly purified human poly-IgG. The universality of the weak interactions suggest that they may contribute to effector function cooperativity in the normal immune response, and we postulate that the generality of the interactions allows for a broader range of epitope spacing for complement activation. These studies demonstrate the utility of analytical ultracentrifuge fluorescence detection in measuring weak protein–protein interactions. It also shows the strength of global analysis of sedimentation velocity data by SEDANAL to extract hydrodynamic nonideality $k_s$ to characterize weak macromolecular interactions.**

**Keywords: human IgG; macromolecular interactions; cooperativity; analytical ultracentrifugation; fluorescence detected sedimentation; sedimentation velocity; hydrodynamic nonideality**

## Introduction

Detecting and characterizing intermolecular interactions in high concentration solutions is important for understanding physiological system behavior, as well as being critical for optimizing drug development processes.[1–3] Significant contributors to intermolecular interaction energies at high concentrations include electrostatics, hydrogen bonding, hydrophobic surfaces, van der Waals attraction and repulsion.[4,5] These interactions are nonspecific and arise from the global properties of the macromolecule such as net charge, dipole or multipole moments, polarity of surface residues, and macromolecular shape.[6,7] The interactions can be either repulsive (steric, electrostatic) or attractive (electrostatic, hydrophobic). All of them are short-ranged (typically, $<1$ nm), with each type of interaction exhibiting its own distance dependence,[5,7] and all are system properties dependent on buffer composition and temperature.[8,9] At high concentrations, when the macromolecules are close to each other, these interactions are manifested in thermodynamic nonideality, solubility, and viscosity. In a practical sense, "high concentration" refers to any concentration where dilute solution approximations no longer describe the experimental data adequately. Studies of nonideal behaviors of macromolecules in concentrated solutions have been a challenge because it is difficult to pinpoint the contributions from each type of interaction to the overall behaviors of the system.

In the biopharmaceutical industry, high-dose monoclonal antibody (mAb) therapies require high-concentration formulations ($>100$ mg/mL) to achieve a sufficiently small injection volume ($<1.5$ mL) for subcutaneous administration.[10] The development of concentrated mAb formulations presents several challenges to analytical characterization due to nonideal behavior, as well as to manufacturing and delivery due to high viscosity, and long-term stability due to self-association and aggregation.[10–12] Within the lifespan of a therapeutic mAb, not only does it experience challenges during drug development, it encounters additional challenges upon administration due to exposure to different sets of system variables. For example, after injection the macromolecular complexity of the system increases dramatically from being a single component in the syringe to encountering the variety of high concentration macromolecular species found in blood.[13,14] Likewise, for any injection, the nature and variety of the surfaces encountered changes dramatically from container surfaces to cell surfaces. Describing the behavior of a molecule undergoing these changes require new models and methods for testing those models.

Molecular crowding models, in which an "effective excluded volume" is used to account for the interactions between molecules, are inadequate for complex solutions. The problem is that the effective excluded volume will depend on the electrostatic features of the adjacent molecules, with repulsion between molecules increasing the effective volume and attraction decreasing it.[5,7] In such mixtures there is no single effective excluded volume. Furthermore, it is not yet clear that an average effective volume can be determined, or if it would be a useful value if it could be determined. Therefore, new means to investigate protein behavior in both homogeneous and heterogeneous, high-concentration, nonideal solutions are required. Having these abilities is not only essential for the development of stable, high-concentration formulations, but they also will contribute understanding of interactions in the very biological systems where mAbs exert their therapeutic effects.

To advance our understanding of intermolecular interactions in IgGs, a series of tracer sedimentation velocity experiments were conducted at serum IgG concentrations. Pairwise interactions were characterized between IgGs differing in subclass and epitope specificity. To carry out these experiments, a panel of seven fluorescently labeled tracer IgGs, differing in variable (V) and constant (C) region sequences, were sedimented in increasing concentrations of unlabeled IgGs of identical, similar, and different backgrounds. In the concentrated solution environment, hydrodynamic nonideality arises due to the displacement of solvent by the sedimenting macromolecule, resulting in a "backflow" that impedes the sedimentation of the macromolecule.[15]

This backflow is impacted by excluded volume and charge effects, and it increases with the total concentration of macromolecules.[16,17] Determination of the concentration dependence of sedimentation yields a set of hydrodynamic nonideality coefficients ($k_s$), each of which describes the extent of nonideality for a pairwise interaction. To gain further insight into the nature of the pairwise interactions, some $k_s$ values were determined at different salt concentrations and temperature.

SEDANAL was used to extract self-, $k_{s,ii}$, and cross-, $k_{s,ij\ (i\neq j)}$, hydrodynamic nonideality terms by global analysis of sedimentation velocity data. We will discuss how these pairwise terms may be used to compare the strength of intermolecular interactions among the mAb IgG subclasses. Additional studies were conducted to estimate $k_s$ in solutions of purified human poly-IgGs. By performing quantitative hydrodynamic analysis of therapeutic mAbs in complex, crowded environments, we seek to clarify the effects of nonideality on weak interactions between IgG molecules, and propose a model to explain the associative interactions under nonideal high concentration conditions.

## Theory

### *Fluorescence detected sedimentation*

Sedimentation velocity analytical ultracentrifugation, SV-AUC, is a mass transport method that provides first principle thermodynamic and hydrodynamic properties of the macromolecule based on rates of sedimentation and boundary spreading in a centrifugal field.[18–20] The discrimination provided by the fluorescence detection systems (FDS) allows the sedimentation behavior of a trace quantity of a labeled molecule to be determine in complex, concentrated solutions such as serum.[21–24] The current work uses FDS to monitor the sedimentation of specific fluorescently labeled IgG molecules under physiologically relevant IgG concentrations, salt concentration, and pH conditions.

### *Analysis of nonideal sedimentation velocity*

The analysis of SV data in solutions of high macromolecular concentration requires consideration of both hydrodynamic and thermodynamic nonideality.[25,26] Hydrodynamic nonideality slows and sharpens a sedimenting boundary in a concentration-dependent manner, and largely arises from the solvent backflow needed to replace the space occupied by the sedimenting macromolecules. Several factors affect the backflow, including the shape of the macromolecule and its interaction with other species (both small- and macromolecules) in the solution.[27] All ion flows are complicated by the need to maintain solution electroneutrality over short (<1 nm) distances. This complication is mitigated by using a high concentration of highly mobile solvent ions ($>50 \times 10^{-3}\ M$) to compensate for the macro-ion sedimentation ($<2 \times 10^{-3}$ N). Nonetheless, all species flows are coupled, complicating the analysis and interpretation of sedimentation in complex, concentrated solutions, and necessitating the use of simplifying assumptions. One of these assumptions is that the solvent may be treated as a single thermodynamic component that maintains solution electroneutrality throughout the sedimentation process. In the context of AUC, treatment of the solvent as a single component implies that any concentration adjustment of a solvent component needed to maintain its constant chemical potential across a sedimenting boundary will not impact the experimental data. In the experiments reported here, the concentration adjustments are small relative to the total component concentrations. With this assumption, only the coupling of flows between macromolecules needs to be considered.

By far, the greatest contribution to the coupled flow is macromolecular size and concentration. Simply put, the greater the volume of sedimenting macromolecules, the more solvent must flow to replace the sedimenting macromolecule. The force generated by the solvent backflow is added to the force due to gradient of the centrifugal potential (i.e., the driving force for sedimentation) and the force created by the gradient of the chemical potential (i.e., the driving force for diffusional transport).[27–29] Because the extent of solvent backflow is proportional to the macromolecular concentration, the backflow increases across a sedimenting boundary. The result is that molecules ahead of the boundary move more slowly than those behind the boundary, which leads to a decrease in the sedimentation coefficient (s), as well as a decrease in boundary spreading. It is important to note that in high-concentration systems, s is not a constant, but varies with radial position (due to boundaries) and time (due to radial dilution).

For a two-component system (macromolecular plus solvent) hydrodynamic nonideality is accounted for by the concentration dependence of the frictional coefficient:

$$f = f^0(1 + k_s c) \tag{1}$$

where $f^0$ is the frictional coefficient at infinite dilution. Thermodynamic nonideality is driven by the concentration dependence of the activity coefficient, $\gamma$:

$$\left(1 + \frac{\partial ln\,(\gamma)}{\partial ln\,(c)}\right) \tag{2}$$

Nonideality from both sources is incorporated into the concentration dependence of the sedimentation

coefficient, $s(c)$, and the concentration dependence of the diffusion coefficient, $D(c)$, expressed as:

$$s(c)=\frac{s^0}{(1+k_s c)} \tag{3}$$

$$D(c)=D^0\frac{\left(1+c\frac{\partial ln\,(\gamma)}{\partial(c)}\right)}{(1+k_s c)} \tag{4}$$

where $s^0$ and $D^0$ are the values of s and D at infinite dilution, respectively. It should be noted that, according to Eq. (3), the sedimentation coefficient, revealed by the position of a boundary in the cell, is independent of thermodynamic nonideality. This is not to say that $k_s$ is independent of thermodynamic considerations, but that $k_s$ is manifested in the boundary position. It is the shape of the boundary, where diffusion is evident, that reveals both thermodynamic and hydrodynamic nonideality. It is noteworthy, too, that both sedimentation and diffusional transport processes experience backflow proportional to the hydrodynamic volume of the macromolecules being transported, regardless of differences in the type of force driving the transport of the macromolecule. It has been established that at infinite dilution, the frictional coefficients for sedimentation and diffusion are equal, and that expressing the concentration dependence as $(1+\boldsymbol{k_s c})$ applies over a wider concentration range than alternative approximations.[30] Stafford showed recently that $(1+\boldsymbol{k_s c})$ should be used in both equations.[15] Therefore, any difference in the concentration dependence of s and D arises solely from the thermodynamic nonideality term.[31] For a two component system, the concentration dependence of the activity coefficient is represented by a power series (i.e., virial expansion) that is truncated after the first-order term:

$$ln\,\gamma=2BMc+0c^2\ldots \tag{5}$$

$$\frac{\partial ln\,\gamma}{\partial c}=2BM \tag{6}$$

where $B$ is the second virial coefficient, $M$ is the molecular weight of the macromolecule, and $0\boldsymbol{c}^2\ldots$ refers to the truncated higher order virial coefficient terms.

$$\text{Substituting}\left(1+\frac{\partial ln\,(\gamma)}{\partial ln\,(c)}\right)=(1+2BMc) \tag{7}$$

Equation (4) becomes:

$$D(c)=D^0\frac{(1+2BMc)}{(1+k_s c)} \tag{8}$$

The factor $(1+k_s c)$ represents the concentration dependence of the sedimentation coefficient, whereas the factor $(1+2BMc)$ represents the contribution from thermodynamic nonideality.

For a three-component system (two macromolecular components plus solvent), the effect of one macromolecular component on another may be determined by monitoring the sedimentation of a trace quantity of a labeled component in a concentration series of unlabeled background component. The factors that represent the hydrodynamic nonideality and thermodynamic nonideality in Eq. (8) need to be expanded in order to account for both sedimenting species: $\left(1+k_{s,ii}c_i+\sum_{j=1,j\neq i}^{n}k_{s,ij}c_j\right)$ and $\left(1+2B_{ii}M_i c_i+2\sum_{j=1,j\neq i}^{n}B_{ij}M_j c_j\right)$, respectively. The cross-term describing the interaction between the heterogeneous species is $k_{s,ij}$, while $k_{s,ii}$ describes the self-interaction. Since the concentration of the labeled tracer species, $I$, is low (100 n$M$, ~0.015 mg/mL) compared to the unlabeled background species $j$ (1–20 mg/mL), the $k_{s,ii}c_i$ and $2B_{ii}M_i c_i$ terms for the tracer component can be neglected. Therefore for $n$ components Eqs. (3) and (8) become:

$$s_i(c_j)=\frac{s_i^0}{\left(1+\sum_{j=1}^{n}k_{s,ij}c_j\right)} \tag{9}$$

$$D_i(c_j)=D_i^0\frac{\left(1+2B_{ii}M_i c_i+2\sum_{j=1,j\neq i}^{n}B_{ij}M_j c_j\right)}{\left(1+\sum_{j=1}^{n}k_{s,ij}c_j\right)} \tag{10}$$

From Eq. (3), values of $k_s$ may be determined empirically from the slope of a plot of inverse weight-average sedimentation coefficient, $\frac{1}{s_w}$, versus loading concentration. However, as noted above, s is not constant with radial position or time, resulting in some ambiguity as to how $s_w$ should be determined. A far better approach is to use recently developed features in the analysis program, SEDANAL, to fit sedimentation data from several experiments conducted at different loading concentrations of homogeneous (i.e., tracer $i$ sedimenting in its unlabeled background) and heterogeneous (i.e., tracer $i$ sedimenting in unlabeled $j$ background) solutions to extract global values of $k_{s,ii}$ and $k_{s,ij}$, respectively. The nonideal model constructed with the ModelEditor in SEDANAL includes a series of parameters described in Eq. (8). These parameters can be constrained or "floated" in a fit. Furthermore, the parameters themselves may be linked to other parameters through assumptions about their relationships. For example, there may be relationships between the parameters describing the sedimentation of non-interacting monomer and dimers ($s(2)=1.4\cdot s(1)$), or the weight concentration extinction coefficients may be assumed to be constant for homo-oligomers or aggregates ($e(2)=e(1)$).[16]

**Table I.** *pI and $Z_{DHH}$ for mAbs and Human IgG*

| ID | Subclass | pI | | | $Z_{DHH}$ | |
|---|---|---|---|---|---|---|
| | | Acidic peak | Main peak | Basic peak | pH 5 Acetate | pH 7.4 PBS |
| Human IgG | | see Figure 1 | | | 0 | $-6.3 \pm 0.2$ |
| mAb1 | IgG1 | 7.9 | 8.1 | 8.2 | $7.7 \pm 0.2$ | $-5.6 \pm 0.1$ |
| | IgG4Pro | 6.2 | 6.3 | 6.5 | $1.4 \pm 0.8$ | $-13 \pm 0.3$ |
| mAb2 | IgG1 | 8.2 | 8.4 | 8.6 | $10.6 \pm 0.1$ | 0 |
| | IgG4Pro | 7.4 | 7.6 | 7.7 | $5.6 \pm 0.2$ | $-9.6 \pm 0.4$ |
| mAb3 | IgG1 | 8.2 | 8.4 | 8.6 | $12.5 \pm 0.1$ | $-5.3 \pm 0.5$ |
| | IgG4Pro | 7.5 | 7.6 | 7.8 | $7.8 \pm 0.2$ | $-10.7 \pm 0.4$ |

### *Interpretation of $k_s$ based on non-interacting spheres*

Typical magnitudes of $k_s$ for spheres are on the order of 10 mL/g or less, but are larger for asymmetric molecules.[32,33] For compact and non-interacting spherical proteins, $k_s$ is between 4 and 9 mL/g.[32,34–36]

A heuristic understanding of how to interpret $k_s$ with respect to particle-particle interactions relies on the understanding that sedimentation works on average density differences between adjacent volume elements, $s \propto \frac{\partial \rho}{\partial r}$. Values of $k_s > 9$ mL/g indicates that, on average, the density of elements is less than would be expected for non-interacting spheres. This situation is encountered where repulsion between molecules leads to a lower average concentration in a volume element or where molecular asymmetry leads to a greater entrained solvent volume, again leading to a lower average density in the volume element.[25] In contrast, values of $k_s < 9$ mL/g indicate that there are attractive interactions between molecules, leading to a higher average density in the volume element and, therefore, a larger s than anticipated for non-interacting spheres. The nature of the attractive interactions need not be specified—they could be discrete assemblies (e.g., monomer–dimer) or a consequence of preferential macromolecule-macromolecule solvation.

The understanding that for IgGs $k_s > 9$ mL/g indicates protein–protein repulsion or asymmetry, and that $k_s < 9$ mL/g indicates protein–protein attraction is the foundation of our interpretation of $k_{s,ii}$ and $k_{s,ij}$ values.

## Results

### *Characterization of human serum IgGs and mAb IgGs*

The purified IgG samples were evaluated for their monomer content, isoelectric point (pI), and average charge ($Z_{DHH}$ valence). These analyses are important for the interpretation of the nonideality observed subsequently in experiments performed on high solute concentration solutions. SV-AUC analysis on the protein A purified IgGs from human serum shows that the corrected $S_{20,w}$-value for the major component (95%) of human poly IgGs is consistent with a monomeric IgG (Fig. S1). The quality of the mAb IgGs also were evaluated by SV-AUC and the monomer content was found to be >95% (data not shown).

In contrast to distinct pI peaks between ~6 and ~8.5 with mAb IgGs (Table I), no distinct peaks were visible in the human poly IgGs. The isoelectric focusing (IEF) gel image reveals that human IgGs contain diverse charge variants comprising both acidic (<pH 4) and basic (>pH 9) ranges [Fig. 1(A)]. Consistent with this finding is the observation of a broad elution peak from cation exchange chromatography (CEX) obtained over a wide range of salt concentrations [Fig. 1(B)]. It should be noted that not all charge variants in the human IgG sample were captured by the CEX column, consistent with there being IgGs having pIs < 5. Nevertheless, the smeared IEF profile and wide CEX elution boundary are evidence for a high degree of charge heterogeneity in the human IgG sample.

The charge of the human poly IgGs was measured by membrane confined electrophoresis (MCE) in both pH 5 acetate and pH 7.4 PBS solution conditions. Experiments were conducted with the cathode at the cuvette bottom, i.e., looking for cationic protein boundaries, and with the anode at the cuvette bottom, i.e., looking for anionic protein boundaries. No boundary movement could be detected in pH 5 acetate in either field direction, indicating that the human IgGs exhibit a near-neutral charge in this buffer. In contrast, in PBS a boundary was observed that moved towards the anode, indicating that the human IgGs are negatively charged with an average $Z_{DHH}$ of $-6.3 \pm 0.2$ (Fig. S2). As shown in Table I, opposite charge signs are observed between pH 5 acetate (i.e., positive) and pH 7.4 PBS (i.e., negative) for mAb IgGs. While the charge magnitude is less for IgG4Pro than for IgG1 in pH 5 acetate, IgG4Pro is more negatively charged by ~2-fold in $Z_{DHH}$ magnitude in the physiological relevantly pH 7.4 PBS solution.

The quality of each fluorescently labeled IgG was evaluated to ensure material quality after labeling. The molar ratio between the dye and each IgG is in the desired 1–3 range based on the ultraviolet (UV) measurements at the respective dye and protein absorption wavelengths. Each Alexa Fluor (AF)

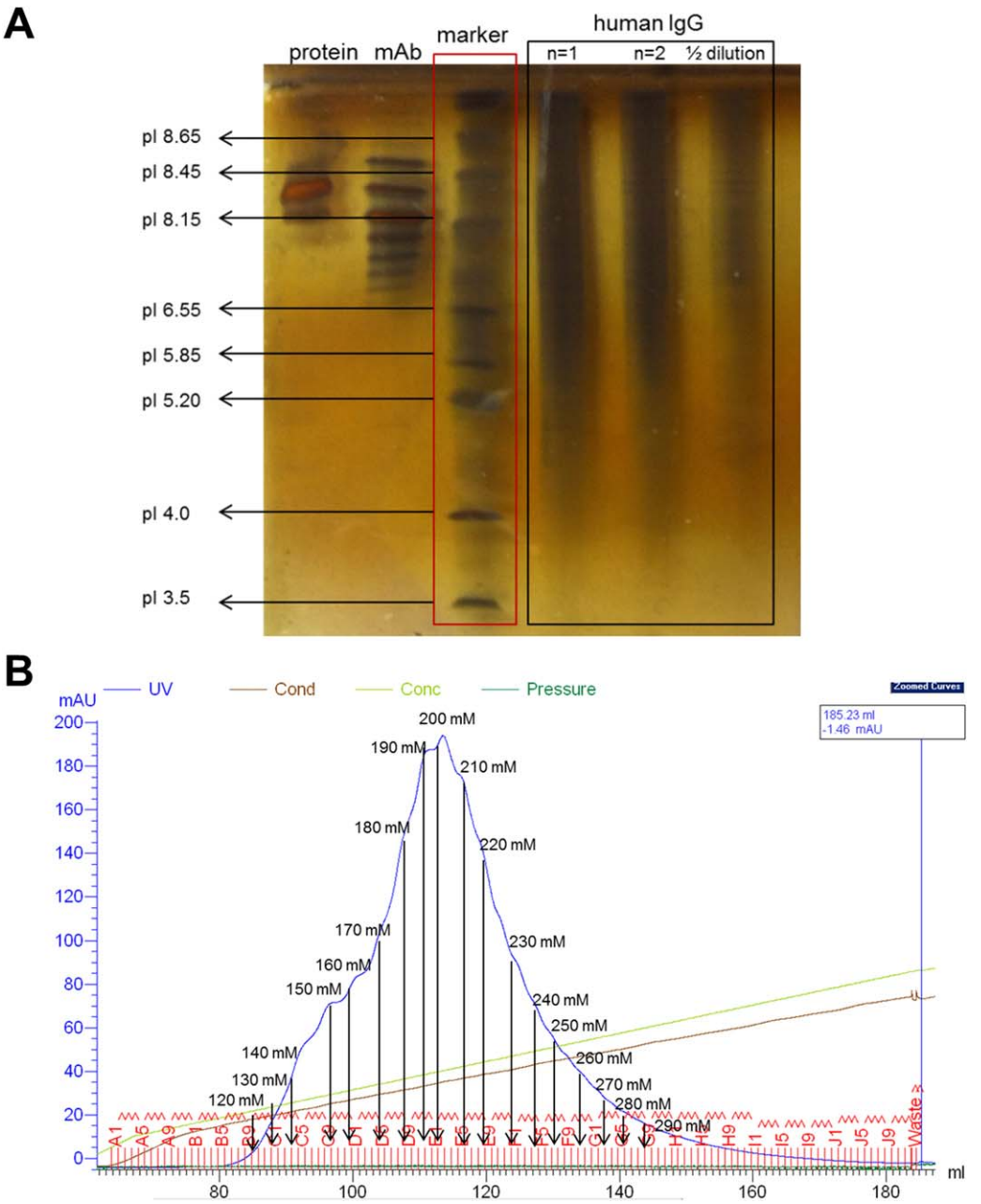


**Figure 1.** Charge variant characterization of human IgGs. (A) IEF gel analysis with three separate loadings of the human IgG sample. A reference mAb and protein were included in the same experiment as controls. (B) CEX chromatogram showing absorbance unit as s function of salt concentration (blue) with conductance (brown) and concentration (yellow) overlaid. The salt concentration is indicated for incremental fractions in the elution profile.

488 labeled IgG was analyzed by SV in PBS in the absence of background molecules at 20°C. An example of the raw SV-AUC data collected by FDS is shown in Figure 2(A). Only a single boundary, moving at a rate consistent with IgG sedimentation, is observed, indicating the AF488 label remains attached to the IgG over the course of the experiment. Figure 2(B) shows an example of the quality of data fit to a two-component model in SEDANAL with the results summarized in Table II. The $S_{20,w}$ values are consistent with IgG monomer being the predominant species. Overall, the AF488 labeled IgG mAbs and human IgGs are comparable in shape and size, as expected.

### $k_{s,ii}$ *determination from sedimentation velocity*

The sedimentation profiles of AF488 labeled human IgG as a function of various background loading concentrations is shown in Figure 3(A). With increasing concentration from 1 to 20 mg/mL, the sedimentation boundary moves slower and sharpens as the hydrodynamic nonideality starts to dominate the process. To obtain the self-nonideality $k_{s,ii}$ term, a two component (non-interacting monomer and

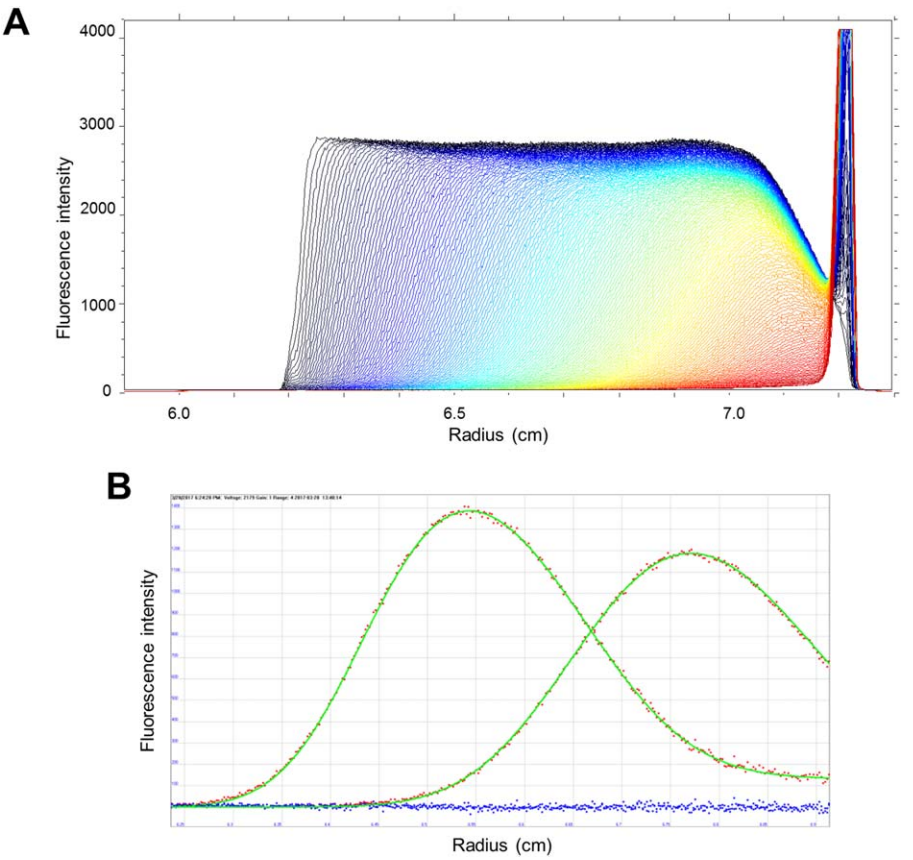


**Figure 2.** Characterization of AF488 labeled tracer IgGs by sedimentation velocity. (A) Raw sedimentation velocity data for 100 n*M* human IgG in pH 7.4 PBS from 200 intensity scans collected at 40,000 rpm at 20°C. SEDFIT was used to visualize the data. The change in color gradient represents the sedimentation of IgG from the top of the cell to the bottom of the cell. (B) Analysis of sedimentation velocity data to a two component model using SEDANAL. The two curves in each panel represent the transformed g(s*) distribution using the first and the last pairs of chosen sedimentation scans through time derivative (dc/d*t*)*r* at each radial position. The overlaid lines (green) over the raw data (red) are the best fitted curves from the model and the fit residuals (blue) are shown at the bottom.

dimer) nonideal model was selected to fit the data, with fixed values for M and s determined from the IgG tracer data. A fixed partial specific volume ($\bar{v}$) of 0.73 mL/g was used (The assumption that $\bar{v}$ is independent of the solution may be in error for high-concentration systems. The error arises from the fact that $\bar{v}$ is the volume of solution displaced per gram of IgG added to the solution (at constant chemical potential of all other components), and its value may change if preferential solvation/hydration by solution components exists. The available data on the protein-concentration-dependence of $\bar{v}$ suggest that its value decreases with increasing concentration, though not by a great amount.[37]). The thermodynamic nonideality term, *BM*, was constrained using the measured B ($1 \times 10^{-5}$ mL-mol/g$^2$) and M (144,000 g/mol) values from the NIST mAb.[38] In addition to $k_s$, the meniscus position and the loading concentrations ($c_{expected}$) of the two components were allowed to float during the fitting process. In all

**Table II.** *Properties of AF488 Labeled IgG in pH 7.4 PBS at 20°C*

| Tracer IgG | Degree of labeling $mol_{dye}/mol_{Ab}$ | Molecular properties | | |
|---|---|---|---|---|
| | | $S_{20,w}$ | $M_W$ (kDa) | Monomer (%)[a] |
| mAb 1 IgG1 | 2.2 | 6.84 | 148 | 98.3 |
| mAb 1 IgG4Pro | 1.3 | 6.83 | 147 | 99.6 |
| mAb 2 IgG1 | 2.6 | 6.76 | 147 | 99.4 |
| mAb 2 IgG4Pro | 1.5 | 6.81 | 148 | 99.7 |
| mAb 3 IgG1 | 1.7 | 6.77 | 149 | 99.9 |
| mAb 3 IgG4Pro | 1.6 | 6.85 | 152 | 99.8 |
| Human IgG | 1.4 | 6.72 | 142 | 99.8 |

[a] Calculated based on the fitted concentrations of the two components.

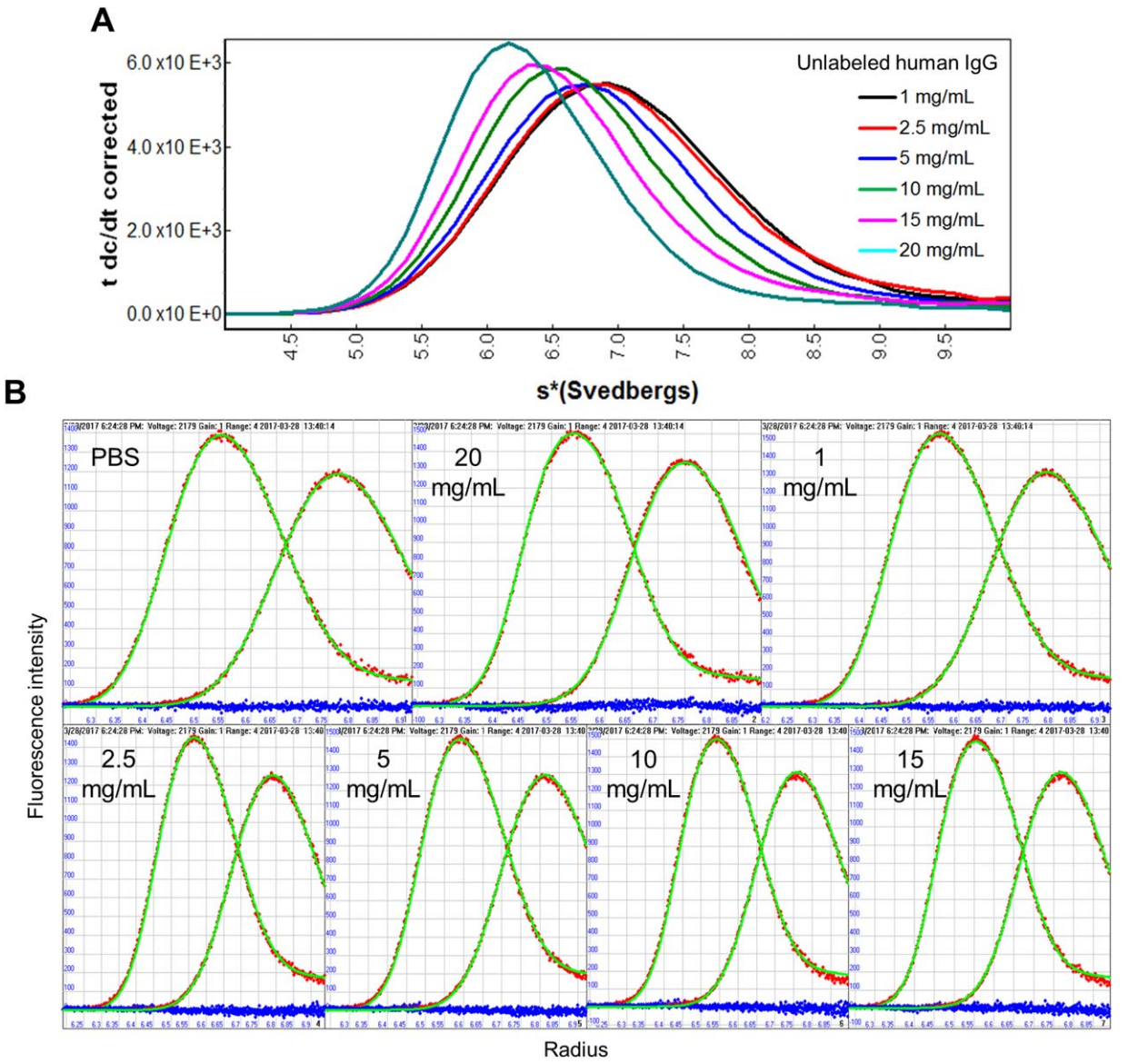


**Figure 3.** Characterization of AF488 labeled human IgG in increasing concentration of self-background solutions. (A) Sedimentation profiles of 100 n*M* human IgG as a function of concentration in pH 7.4 PBS at 20°C. The plots were generated in SEDVIEW where the *y*-axis *t*·dc/d*t* corrected is essentially *s*·*g*(*s**) after correcting for radial dilution. The peak position represents the *s**-value. (B) Global analysis of sedimentation velocity data using SEDANAL. The transformed *g*(*s**) curves from the first and last pairs of scans are plotted as intensity versus radius in each panel corresponding to the background concentration. The overlaid lines (green) over the raw data (red) are the best fitted curves from the model and the fit residuals (blue) are shown at the bottom. The best fit $k_s$ parameters are: $k_{s,ii} = 5.1$ mL/g; best fit std. dev. = 11.0 after 30 iterations. The constrained parameters are: MW = 1.44 × 105 g/mol; $s = 6.5$ S; density increment = 0.27 (from $\bar{\nu} = 0.73$ mL/g); BM = 1.44 mL/g as explained in the text.

cases, $c_{fit}/c_{expected} = 1.0 \pm 0.1$, with one exception where $c_{fit}/c_{expected} = 0.8$. The resulting SEDANAL fitting analysis is shown in Figure 3(B). An overlay of the data with the model fit indicates that the concentration dependence of sedimentation fit well to the chosen two component nonideal model for all the concentrations.

To assess the reproducibility of the data and the robustness of the fitted $k_{s,ii}$ value, separate experiments were conducted using five fresh samples of human IgG tracer in increasing concentration of unlabeled human poly IgG. Identical sample preparations, experimental conditions, and data analysis procedures were applied. The fitted $k_{s,ii}$ values (in mL/g unit) are 5.1, 4.8, 4.6, 5.1, and 5.2, yielding an average of $5.0 \pm 0.3$. Furthermore, the goodness-of-fit and the confidence limits of fitted parameters were determined by a "bootstrap with replacement" analysis with 10 bootstrap fitting operations.[31] The results show identical $k_{s,ii}$ values between the

**Table III.** *Sensitivity Analysis for the Two Component Nonideal Model*

| $B \times 10^{-5}$ (mL-mol/g$^2$) | BM (mL/g) | $k_{s,ii}$ (mL/g) | Deviation[a] |
|---|---|---|---|
| 0.1 | 0.14 | 4.9 | 0.1 |
| 0.5 | 0.72 | 4.8 | 0.2 |
| 1 | 1.44 | 4.8 | 0.2 |
| 2 | 2.88 | 5.0 | 0.0 |
| 5 | 7.20 | 5.3 | 0.3 |
| 10 | 14.4 | 5.7 | 0.7 |

[a] Calculated in relation to the average $k_{s,ii}$ of 5.0.

bootstrap fits, indicating that the model adequately explains the data, and that the global analysis represents the data satisfactorily (Table SI).

The sensitivity of $k_{s,ii}$ to the thermodynamic nonideality (BM) was assessed by varying the second virial coefficient (B) while keeping other parameters constant. The results show that the changes in $k_s$ fall within the standard deviation of 0.3 up to $5 \times 10^{-5}$ mL-mol/gm$^2$ (Table III). Only when B was increased by an order of magnitude (i.e., from $1 \times 10^{-5}$ to $10 \times 10^{-5}$ mL-mol/gm$^2$) did the fitted $k_{s,ii}$ become significantly different. This finding suggests that although B was not measured for each IgG, the deviation from the NIST mAb value has little to negligible influence on the fitted $k_s$ within the current set of IgG samples.

### $k_{s,ii}$ *and* $k_{s,ij}$ *from various IgG backgrounds*

A series of FDS experiments were performed to generate the self-nonideality, $k_{s,ii}$, and cross-nonideality, $k_{s,ij}$ terms. In each of these experiments the concentration of the AF488 labeled tracer IgG (species i) was held constant while the unlabeled IgG (species i or j) was titrated over a range of concentrations. SEDANAL was used to analyze the sedimentation profiles of tracer IgG in identical, similar, or different IgG backgrounds. For *identical backgrounds* the background IgG is the same as the tracer IgG. For *similar backgrounds* the background IgG and tracer have identical V-regions, but differ in subclass. For *different backgrounds* both the tracer and background IgGs differ in V-region and subclass (this group includes all mixtures that include the human poly IgGs).

Consistent with the previous observation [Fig. 3(A)], a gradual decrease in apparent sedimentation coefficient, $s^*$, with increasing background concentration is observed for all mixtures. However, the magnitude of the reduction in $s^*$ differs for different backgrounds. An example is shown in Figure 4 for the mAb 1 IgG1 tracer sedimented in different backgrounds at 1 mg/mL (panel A) or at 20 mg/mL (panel B). While $s^*$ is indistinguishable in the different backgrounds at 1 mg/mL, at 20 mg/mL distinct differences in the decrease $s^*$ are apparent. Keeping in mind that greater attraction between proteins leads to smaller decreases in $s^*$, the $s^*$ shifts seen in Figure 4(B) suggest that there are stronger attractions between mAb1 IgG1 and human IgG than for either IgG1 or IgG4Pro, which exhibits the weakest attraction. These qualitative observations are quantified by fitted determinations of both the self-$k_{s,ii}$ and cross-$k_{s,ij}$ nonideality terms using SEDANAL.

The same nonideal model, macromolecular parameters, and procedure for fitting $k_{s,ii}$ described

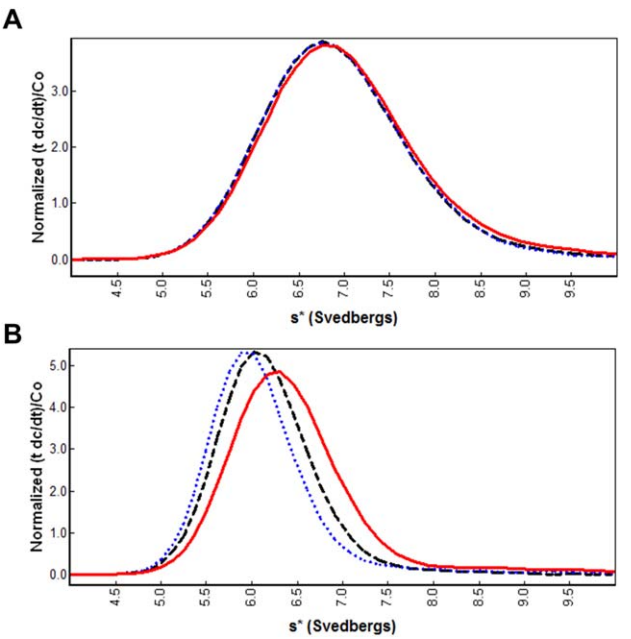


**Figure 4.** Sedimentation profiles of mAb 1 IgG1 in the presence of (A) 1 mg/mL and (B) 20 mg/mL IgG background containing IgG1 (black dashed), IgG4Pro (blue dotted), and human IgG (red solid) in pH 7.4 PBS at 20°C. The plots were generated in SEDVIEW as described in Figure 3.

**Table IV.** *$k_s$ Terms (in mL/g) Mixtures of IgG1, IgG4Pro, and Human IgG Across Three mAb Groups*[a]

| | | Background | | |
|---|---|---|---|---|
| mAb ID | Tracer | IgG1 | IgG4Pro | Human IgG |
| mAb 1 | IgG1 | 7.0 ± 0.4 | 8.0 ± 0.4 | 4.3 ± 0.2 |
| | IgG4Pro | 8.4 ± 0.4 | 9.1 ± 0.5 | 5.4 ± 0.3 |
| human IgG | | 7.3 ± 0.4 | 8.0 ± 0.4 | 5.1 ± 0.3 |
| mAb 2 | IgG1 | 5.2 ± 0.3 | 5.3 ± 0.3 | 3.2 ± 0.2 |
| | IgG4Pro | 5.5 ± 0.3 | 5.6 ± 0.3 | 4.4 ± 0.2 |
| human IgG | | 6.2 ± 0.3 | 6.5 ± 0.3 | 5.1 ± 0.3 |
| mAb 3 | IgG1 | 6.4 ± 0.3 | 7.5 ± 0.4 | 4.5 ± 0.2 |
| | IgG4Pro | 6.0 ± 0.3 | 8.3 ± 0.4 | 5.1 ± 0.3 |
| human IgG | | 7.2 ± 0.4 | 8.6 ± 0.4 | 5.1 ± 0.3 |

Note IgG1 is referred to as component 1, IgG4Pro as component 2, and human IgG as component 3. The matrix is labeled $k_{s,11}$, $k_{s,12}$, and $k_{s,13}$ across the row, and $k_{s,11}$, $k_{s,21}$, and $k_{s,31}$ through the column. The self-nonideality is labeled $k_{s,11}$, $k_{s,22}$, and $k_{s,33}$ diagonally. The values that are close to ~9 mL/g are marked with superscript.
[a] A 5% standard deviation was applied.

above were used to fit for either the self, $k_{s,ii}$, or cross, $k_{s,ij}$, nonideality terms. Global analysis of data from 27 experiments, including 9 self-nonideality and 18 cross-nonideality evaluations, are in the Figures S3–S9. No systematic residuals are observed between the apparent sedimentation coefficient distribution function, g(s*), and the fit, indicating that the model reproduces the data adequately.

The full set of the self- and cross- nonideality terms derived from these global analyses is summarized in Table IV. The data shows that the measured $k_s$ values range from as low as 3.2 (greatest attraction) to as high as 9.1 (no attraction). It appears that the V region impacts the strength of the attraction. Comparison of the self ($k_{s,ii}$) values for the three mAb V-regions reveals that mAb 2 exhibits the strongest self-attraction ($k_{s,11} = 5.2$ and $k_{s,22} = 5.6$), followed by mAb 3 ($k_{s,11} = 6.4$ and $k_{s,22} = 8.3$), while mAb 1 has the weakest attraction ($k_{s,11} = 7.0$ and $k_{s,22} = 9.1$) for both IgG1 and IgG4Pro subclasses. In addition, the observation that the self-nonideality term is lower for IgG1 than for IgG4Pro suggests that the IgG1 C region may have stronger endogenous self-associative traits than IgG4Pro.

Comparison of the cross-nonideality terms within the 3 × 3 matrix for each mAb group also reveals variations in the $k_{s,ij}$ values, suggesting that the magnitude of weak associative interactions is pairwise specific. Notably, the $k_{s,ij}$ values for the human IgG background are not only ~2-fold less than the minimum nonideality value of 9 mL/gm (Section 2.3), but also are lower compared to those of identical or similar backgrounds within each mAb group, suggesting that human IgG exhibits stronger interaction with the mAb IgGs than mAb IgGs exert upon themselves. Since the human IgG's magnitude of self-association ($k_{s,33} = 5.1$) is comparable to that of its cross-association for mAb IgGs (average $k_{s,13/23} = 4.7 \pm 0.7$), but at a lower strength compared to the self-association of each of the IgG1 and IgG4Pro subclasses in both mAb 1 and mAb 3, it appears that the observed increased associative interaction is due to human IgG having the greatest endogenous self-association attribute.

It is noteworthy that although both IgG1 and IgG4Pro subclasses in mAb 2 exhibit identical magnitudes of endogenous self-association as human IgG, human IgG nonetheless exerts even stronger associative interaction upon both subclasses ($k_{s,13} = 3.2$ and $k_{s,23} = 4.4$). Conversely, the associative effect that human IgG exerts on mAb IgGs is not reciprocal. When mAb IgGs are in excess in the background, the cross terms are either comparable to the minimum nonideality value ($k_{s,32} = 8.6$ in mAb 3) or to the self-association of the mAb IgG ($k_{s,31} = 7.3$ in mAb 1). Together, these observations serve as evidence that the enhancement of weak attractive interactions between IgG molecules is caused by human IgG's natural ability to self-associate, resulting in masking of the cross-term nonideality. The results also suggest that the weak attractions are promiscuous.

Comparison of the pairwise interactions between IgG1 and IgG4Pro reveals that the nonideality effects are different across the mAb groups. In mAb 1, the cross terms are not only symmetric ($k_{s,12} = 8.0$ and $k_{s,21} = 8.4$) but also are comparable to the 9.0 mL/g minimum for non-interacting spheres (above), suggesting that any attraction is very weak. Similarly, the cross terms are symmetric in mAb 2 ($k_{s,12} = 5.3$ and $k_{s,21} = 5.5$) suggest stronger, reciprocal, attraction between them. On the other hand, $k_{s,ij}$ for mAb 3 IgG1 and IgG4Pro are not equal ($k_{s,12} = 7.5$ and $k_{s,21} = 6.0$), suggesting that there is a stronger attraction when IgG1 is the background. Since IgG1 has stronger endogenous self-association (i.e., lower $k_{s,ii}$) than IgG4Pro, it suggests that IgG1 exerts stronger associative effect on IgG4Pro than IgG4Pro does upon itself.

### *Modulation of $k_s$ by salt concentration and temperature*

IgG4Pro $Z_{DHH}$ is ~2-fold more negatively charged than IgG1 in pH 7.4 PBS, 150 m*M* NaCl (Table I).

**Table V.** *Effect of Salt Concentration on $k_s$ (in mL/g) in pH 7.4 PBS at 20°C. A 5% Standard Deviation was Applied*

| NaCl concentration | Tracer | Background | | |
|---|---|---|---|---|
| | | IgG1 | IgG4Pro | Human IgG |
| 150 m*M* | mAb3 IgG1 | 6.4 ± 0.3 | 7.5 ± 0.4 | 4.5 ± 0.2 |
| | mAb3 IgG4Pro | 6.0 ± 0.3 | 8.3 ± 0.4 | 5.1 ± 0.3 |
| | Human IgG | n.d. | n.d. | 5.1 ± 0.3 |
| 500 m*M* | mAb3 IgG1 | 8.4 ± 0.4 | 8.7 ± 0.4 | 6.9 ± 0.3 |
| | mAb3 IgG4Pro | 8.0 ± 0.4 | 8.2 ± 0.4 | 7.3 ± 0.4 |
| | Human IgG | n.d. | n.d. | 7.6 ± 0.4 |

n.d. not determined.

Together with the findings that the pairwise interaction is weaker (i.e., higher $k_{s,ij}$) in the IgG4Pro background than in the IgG1 background in mAb 3, it might be postulated that the higher $Z_{DHH}$ valence is the primary reason for the attenuation of the attractive intermolecular interaction observed in IgG4Pro. To test this hypothesis, the ionic strength of the PBS buffer was increased with the addition of 500 m*M* NaCl to further screen the electrostatic interactions. If attractive electrostatic interactions (e.g., charge-dipole, dipole–dipole) are significant contributors to the differences in $k_{s,ij}$, increasing the ionic strength will weaken them and $k_{s,ij}$ will increase. Conversely, increased salt will decrease $k_{s,ij}$ if repulsive electrostatic interactions (charge-charge) interactions are significant. Determining the impact of higher salt, then, may help elucidate the contribution of electrostatics to the interactions.

Using mAb 3 and human IgG as examples, the results summarized in Table V show increases in both the $k_{s,ii}$ and $k_{s,ij}$ values with increased NaCl, indicating a reduction in the strength of attractive intermolecular electrostatics are more important than charge-charge repulsion. In support of this interpretation, despite the large valence difference between IgG1 and IgG4Pro in mAb 2 ($Z_{DHH} = 0$ for IgG1 and $Z_{DHH} = -9.6$ for IgG4Pro), the self and cross terms are indistinguishable (see Table IV). Based on the charge differences, differences in $k_s$ would have been anticipated for these two subclasses if repulsive electrostatics were significant.

**Table VI.** *Effect of Temperature on $k_s$ (mL/g) Determined from Sedimentation in the Human IgG Background in pH 7.4 PBS 150 mM NaCl. A Standard 5% Standard Deviation was Applied*

| Tracer | 10°C | 20°C |
|---|---|---|
| Human IgG[a] | 3.2 ± 0.2 | 5.1 ± 0.3 |
| mAb 1 IgG1 | 3.7 ± 0.2 | 4.3 ± 0.2 |
| mAb 1 IgG4Pro | 4.7 ± 0.2 | 5.4 ± 0.3 |
| mAb 2 IgG1 | 2.9 ± 0.1 | 3.2 ± 0.2 |
| mAb 2 IgG4Pro | 3.4 ± 0.2 | 4.4 ± 0.2 |
| mAb 3 IgG1 | 2.8 ± 0.1 | 4.5 ± 0.2 |
| mAb 3 IgG4Pro | 2.7 ± 0.1 | 5.1 ± 0.3 |

[a] Additional experiment was conducted for human IgG at 30°C and the $k_s$ was determined to be 6.0 ± 0.3.

In order to test whether the weak interactions between mAb IgGs are enthalpically or entropically controlled, values of $k_{s,ij}$ were determined for a subset of IgGs at two or three (human IgG) temperatures. The temperature dependence of $k_{s,ij}$ from each of the mAb or human IgG tracer molecules sedimenting in human IgG is shown in Table VI. The consistently higher $k_{s,ij}$ (i.e., attractive interaction weakening) with increasing temperature is consistent with $k_s$ being predominantly enthalpic in origin, and consistent with attractive electrostatic interactions being important.

## Discussion

AU-FDS allows the characterization of interactions between *identical*, *similar*, or *different* IgG molecules through the determination of the hydrodynamic nonideality, $k_s$, in physiologically relevant solvents.

There are three observations that stand out from the results. (1) Even though the human IgG pIs ranged from 4 to 10, the valence ($Z_{DHH}$) for all IgGs fell into a remarkably narrow range near −6.3. These data demonstrate that protein charge must be measured and cannot be estimated from the pI. The narrow valence range suggests that IgG charge is buffered by ion binding concomitant with $H^+$ uptake and release. Gokarn, et al. showed that hen egg white lysozyme binds anions preferentially, which may provide a mechanism for charge buffering.[39] Such buffering may be physiologically relevant in keeping antibody charge within a narrow range over varied conditions (e.g., in secretions or at wound sites). (2) Values of $k_s$ (Table IV) are less than expected for non-interacting spheres. The results using six different IgG mAbs are consistent with there being weak attractive interactions between all IgGs, including human poly-IgG. Values of $k_s$ differ for different IgGs, and both the V and C regions seem to contribute to the differences. Notably, IgG4 generally shows weaker attractive interactions than IgG1, which is consistent with IgG 4's weaker C1q binding/complement activation.[40] The weak attraction between IgGs appears to be indiscriminate. All mAb mixtures exhibited weak attractive interactions

between IgGs, regardless of whether the mixtures were composed of *identical*, *similar* or *different* IgGs, including human poly-IgG.

Cooperative binding is a central feature of biological systems, and IgGs may exhibit any of several cooperative interactions.[41] The observation of indiscriminate, weak attractive interactions between IgGs may have important immunological consequences. Weak attraction between IgGs in solution provides a simple mechanism for cooperative formation of the hexameric C1q binding site on a surface,[42] while avoiding the formation of IgG oligomers and aggregates in serum. Complement activation must be a go/no-go decision, not a maybe-so/maybe-not decision, which could be damaging to the host by depletion of C1q, while resulting simultaneously in an ineffective response to the antigen. Likewise, the indiscriminate nature of the weak attractions may be immunologically important for an effective host response: by having a poly-IgG response, the hexamer can be formed using IgGs that are directed against different epitopes. That is, the hexamer formation does not require there be an "epitope template" consisting of a precisely arrayed single epitope type. Rather, the indiscriminate weak attraction permits any set of epitopes that are arranged properly to allow hexamer formation.

Human adult serum contains high concentrations of serum albumin (~30–40 mg/mL) in addition to IgGs (~10–15 mg/mL) that might impact these results. However, work by Wright et al., using different mAb tracers in mixtures that include albumin show weak IgG:IgG interactions that are consistent with these findings.[43]

## Materials and Methods

### Materials

The 6 mAb IgGs differing in variable regions each constructed in IgG1 and IgG4Pro (IgG4 with S→P mutation in the hinge region) isotypes were provided by Boehringer Ingelheim. Human male AB plasma serum was purchased from Sigma-Aldrich (cat# H4522) and purified with the ÄKTA affinity chromatography system and MabSelect Sure resin (GE Healthcare) following standard methods. Alexa Fluor™ 488 Protein Labeling kits were purchased from Thermo Fischer Scientific (cat# A10235). The mAb IgGs and human IgGs purified from serum were stored in 60 m*M* sodium acetate (pH 5.0) and dialyzed into phosphate-buffered saline (PBS [pH 7.4]: 137 m*M* NaCl, 27 m*M* KCl, 8 m*M* $Na_2HPO_4$, and 1.5 m*M* $KH_2PO_4$) or acetate (10 m*M* acetate [pH 5.0], 50 m*M* NaCl) using Slide-A-Lyzer™ cassettes (Thermo Fischer Scientific, cat# 66380) for the analytical ultracentrifugation experiments. The chemical reagents were analytical grade or better. Water used in the experiments was deionized by a Milli-Q Plus filtration system (Millipore).

### Antibody labeling

Each antibody was diluted to 2 mg/mL in PBS, and 50 μL of 1 *M* sodium bicarbonate was added to the solution. The prepared antibody solution was transferred to a vial of reactive dye (Alexa Fluor 488 carboxylic acid, tetrafluorophenyl ester) and incubated for 1 h at room temperature under mild agitation. The labeled antibody was purified by size exclusion chromatograph (SEC) using BioGel P-30 purification resins (Bio-Rad Laboratories) following protocols provided in the kit. The antibody and free dye bands were detected by illumination with a handheld UV lamp. The concentration of the purified labeled antibody was determined in a SoloVPE UV-Vis spectrophotometer (C Technologies). The UV spectrum was acquired in a 10-mm pathlength quartz cell between 200 and 600 nm. The labeled antibody concentration and the degree of labeling were calculated using the follow equations:

$$\text{protein concentration (M)} = \frac{[A_{280} - (A_{494} \times 0.11)] \times \textit{dilution factor}}{203,000}$$

$$\text{moles dye per mole protein} = \frac{A_{494} \times \textit{dilution factor}}{71,000 \times \textit{concentration}\,(M)}$$

where $A_{280}$ and $A_{494}$ are the background subtracted sample absorbance at 280 and 494 nm, respectively, 0.11 is a correction factor to account for the absorption of the dye at 280 nm, and 203,000 and 71,000 are the molar extinction coefficient ($cm^{-1}\ M^{-1}$) of a typical IgG at 280 nm and the AF488 dye at 494 nm, respectively.

### Cation exchange chromatography

The purified IgG sample from human serum was loaded at 10 mL/min onto a Poros 50 HS 11 mL column that was pre-equilibrated with 10 column volumes of 50 m*M* sodium acetate (pH 5.0) using an ÄKTA Avant system (GE Healthcare). Following a wash with 10 column volumes of the same buffer, a salt gradient of 0–0.4 *M* NaCl was applied at 4 mL/min to elute the bound IgGs from the column. The purification protocol and the sample elution profile with respect to UV and conductance were monitored using the UNICORN system control software.

### Imaged capillary isoelectric focusing

The isoelectric point (pI) of the mAb IgGs was determined on an iCE3 system (Protein Simple). The pH gradient across a fluorocarbon coated capillary was created by an ampholyte mixture consisted of 44% (v/v) of 1% methylcellulose, 1.25% (v/v) of

pharmalyte 3–10 solution, 3.75% (v/v) μL of pharmalyte 5–8 solution, 1.25% (v/v) of servalyte 9–11 solution, 0.63% (v/v) of pI marker pH 6.14, 0.63% (v/v) of pI marker pH 8.79, 6.3% (v/v) of 200 mM iminodiacetic acid, and 43% (v/v) of water. Each antibody was prepared at 1 mg/mL in deionized water, and 40 μL of the solution was mixed with 160 μL of ampholyte mixture and centrifuged for 5 min. The experiment was run by introducing a potential of 1500 volts for 1 min, followed by a potential of 3000 volts for 20 min. For samples containing highly basic species, 0.63% (v/v) of pI markers pH 7.55 and 0.63% (v/v) of pI marker pH 9.77 were added instead, as well as a shorter focus period of 10 min at 3000 volts was used. The separation was monitored at 280 nm. The obtained data were first reviewed in the iCE CFR software to calibrate the pI values and to select the markers. The data files were then exported to Empower for further analysis using the cIEF processing method.

### *Gel electrophoresis and staining*

The pI and charge heterogeneity of human IgGs from serum was determined on a PhastSystem electrophoresis equipment with PhastGel Dry IEF gels (GE Healthcare). The gels were first rehydrated for 1 hr in 1 mL of rehydration solution consisted of 0.9 g urea, 12% (v/v) of glycerol, 10% (v/v) of 20% CHAPS, 3.8% (v/v) of pharmalyte 8–10.5, 3% (v/v) of servalyte 7–9, 0.7% (v/v) of servalyte 3–10, and 70.5% (v/v) of water. After the preparation of the sample at 0.1 mg/mL in 2% CHAPS, 150 ng was loaded onto the gel. The experiment was run using the Dry IEF 3M Urea (550 Vh) method based on the manufacture's recommendations. The gels were developed using silver staining and were allowed to dry overnight before imaging.

### *Membrane confined electrophoresis*

The valence of the IgGs was measured in a MCE instrument (Spin Analytical). In each experiment, 20 μL of sample prepared at 1 mg/mL was loaded into a $2 \times 2 \times 4$ mm$^3$ quartz cuvette whose ends were sealed with semipermeable membranes with a molecular weight cut-off of 3000 Dalton (Spectra/Por Biotech grade). After placing separate buffer chambers on each end of the membrane to supply a continuous flow of fresh buffer throughout the sample compartment, an electric field was applied (4.3 V/cm for mAb IgG and 19.8 V/cm for human IgGs) longitudinally across the cell. The applied electric field is a function of the applied current, conductivity of the buffer (16.8 mS for PBS), and the cross-sectional area of the cuvette. As the charged molecule moved from one end of the cuvette to the other, the intensity of the moving boundary was measured at 280 nm as a function of distance across the cuvette at 10–20 s time point intervals. The collected data were analyzed in the software supplied by Spin Analytical using the following equations:

$$Z_{eff} = \frac{\mu k_B T}{De}$$

$$Z_{DHH} = Z_{eff} \frac{1+\kappa a}{f(\kappa a)}$$

where μ is the electrophoretic mobility, $D$ is the diffusion coefficient, $e$ is the elementary charge, $k_B$ is Boltzmann's constant, $T$ is the temperature, κ is the inverse Debye length, a is the sum of the Stokes radii of the macromolecule and its counterion. The $Z_{eff}$ is the apparent or reduced charge due to counterion shielding and electrophoretic effects from the Debye–Hückel–Henry cloud. The $Z_{DHH}$ represents the valence of the molecule after adjusting from these solvent effects.

### *Sedimentation velocity analytical ultracentrifugation*

Experiments were performed in an Optima XL-I analytical ultracentrifuge (Beckman Coulter) equipped with fluorescence optics (Aviv Biomedical). Each AF488-labeled tracer antibody was prepared at 100 n$M$ in either self- or non-self IgG backgrounds of increasing concentrations (1, 2.5, 5, 10, and 20 mg/mL). All background samples were dialyzed exhaustively against PBS buffer prior to the addition of the tracer antibody. Samples were loaded into both the sample and reference chamber of the AUC cell assembled with standard double-sector centerpieces and quartz windows. The experiments were conducted at 10 and 20°C using an An60Ti 8-hole rotor spinning at 40,000 rpm. Data were acquired at 20-μm radial increments and averaging five resolutions/scan. The collected sedimentation boundary data from FDS were analyzed using a two component nonideality model in SEDANAL (version 6.6.1).[26] Global fits to multiple concentration datasets were performed to obtain the hydrodynamic nonideality parameter $k_s$.


## Acknowledgements

The authors wish to thank Boehringer-Ingelheim for supporting the doctorate research of Danlin Yang, a portion of which is published here. The authors have no conflicts of interest to declare. This paper is dedicated to the memory of Dr. James A. Stewart, Professor of Biochemistry at the University of New Hampshire.


## References


1. Hall D, Minton AP (2003) Macromolecular crowding: qualitative and semiquantitative successes, quantitative challenges. Biochim Biophys Acta 1649:127–139.

2. Saluja A, Kalonia DS (2008) Nature and consequences of protein–protein interactions in high protein concentration solutions. Int J Pharm 358:1–15.
3. Tomar DS, Kumar S, Singh SK, Goswami S, Li L (2016) Molecular basis of high viscosity in concentrated antibody solutions: strategies for high concentration drug product development. mAbs 8:216–228.
4. Israelachvili JN (2011) Intermolecular and surface forces, 3rd edn. Amsterdam: Academic Press.
5. Laue T, Demeler B (2011) A postreductionist framework for protein biochemistry. Nat Chem Biol 7:331–334.
6. Minton AP (2001) The influence of macromolecular crowding and macromolecular confinement on biochemical reactions in physiological media. J Biol Chem 276: 10577–10580.
7. Laue T (2012) Proximity energies: a framework for understanding concentrated solutions. J Mol Recognit 25:165–173.
8. Fodeke AA, Minton AP (2011) Quantitative characterization of temperature-independent and temperature-dependent protein–protein interactions in highly nonideal solutions. J Phys Chem B 115:11261–11268.
9. Roberts D, Keeling R, Tracka M, van der Walle CF, Uddin S, Warwicker J, Curtis R (2015) Specific ion and buffer effects on protein–protein interactions of a monoclonal antibody. Mol Pharm 12:179–193.
10. Shire SJ, Shahrokh Z, Liu J (2004) Challenges in the development of high protein concentration formulations. J Pharm Sci 93:1390–1402.
11. Harris RJ, Shire SJ, Winter C (2004) Commercial manufacturing scale formulation and analytical characterization of therapeutic recombinant antibodies. Drug Dev Res 61:137–154.
12. Daugherty AL, Mrsny RJ (2006) Formulation and delivery issues for monoclonal antibody therapeutics. Adv Drug Deliv Rev 58:686–706.
13. Scott EM, Waterhouse JM (1986) Physiology and the scientific method. Manchester: Manchester University Press.
14. Adkins JN, Varnum SM, Auberry KJ, Moore RJ, Angell NH, Smith RD, Springer DL, Pounds JG (2002) Toward a human blood serum proteome analysis by multidimensional separation coupled with mass spectrometry. Mol Cell Proteomics 1:947–955.
15. Stafford WF, Analysis of nonideal, interacting, and noninteracting systems by sedimentation velocity analytical ultracentrifugation. In: (2016) Analytical ultracentrifugation. Uchiyama, S, Arisaka, F, Stafford, WF, Laue, T. (Eds.) Tokyo: Springer, pp. 463–482.
16. Cole JL, Correia JJ, Stafford WF (2011) The use of analytical sedimentation velocity to extract thermodynamic linkage. Biophys Chem 159:120–128.
17. Correia JJ, Stafford WF (2015) Sedimentation velocity. Methods Enzymol 562:49–80.
18. McRorie DK, Voelker PJ (1993) Self-associating systems in the analytical ultracentrifugation. Palo Alto, CA: Beckman Instruments.
19. Schuck P (2013) Analytical ultracentrifugation as a tool for studying protein interactions. Biophys Rev 5:159–171.
20. Stafford WF (1997) Sedimentation velocity spins a new weave for an old fabric. Curr Opin Biotechnol 8:14–24.
21. MacGregor IK, Anderson AL, Laue TM (2004) Fluorescence detection for the XLI analytical ultracentrifuge. Biophys Chem 108:165–185.
22. Kingsbury JS, Laue TM, Klimtchuk ES, Théberge R, Costello CE, Connors LH (2008) The modulation of transthyretin tetramer stability by cysteine 10 adducts and the drug diflunisal. Direct analysis by fluorescence-detected analytical ultracentrifugation. J Biol Chem 283:11887–11896.
23. Demeule B, Shire SJ, Liu J (2009) A therapeutic antibody and its antigen form different complexes in serum than in phosphate-buffered saline: a study by analytical ultracentrifugation. Anal Biochem 388:279–287.
24. Kroe RR, Laue TM (2009) NUTS and BOLTS: applications of fluorescence-detected sedimentation. Anal Biochem 390:1–13.
25. Rowe AJ (1977) The concentration dependence of transport processes: a general description applicable to the sedimentation, translational diffusion, and viscosity coefficients of macromolecular solutes. Biopolymers 16:2595–2611.
26. Stafford WF, Sherwood PJ (2004) Analysis of heterologous interacting systems by sedimentation velocity: curve fitting algorithms for estimation of sedimentation coefficients, equilibrium and kinetic constants. Biophys Chem 108:231–243.
27. Fuoss RM, Onsager L (1961) Thermodynamic potentials of symmetrical electrolytes. Proc Natl Acad Sci USA 47:818–825.
28. Katchalsky AK, Curran PF (1967) Nonequilibrium thermodynamics in biophysics. 1st edn. Cambridge, MA: Harvard University Press.
29. Harding SE, Johnson P (1985) The concentration-dependence of macromolecular parameters. Biochem J 231:543–547.
30. Schachman HK (1959) Ultracentrifugation in biochemistry. New York, NY: Academic Press Inc.
31. Sherwood PJ, Stafford WF. SEDANAL: model-dependent and model-independent analysis of sedimentation data. In: (2016) Analytical ultracentrifugation. Uchiyama, S, Arisaka, F, Stafford, WF, Laue, T. (Eds.) Tokyo: Springer, pp. 81–102.
32. Creeth JM, Knight CG (1965) On the estimation of the shape of macromolecules from sedimentation and viscosity measurements. Biochim Biophys Acta Biophys Photosynth 102:549–558.
33. Harding SE, Rowe AJ, Horton JC, editors (1992) Analytical ultracentrifugation in biochemistry and polymer science, 1st edn. Cambridge, England: Royal Society of Chemistry.
34. Teller DC. Methods in enzymology, Vol. XXVII. In: Hirs CHW, Timasheff SN, Eds. (1973) Characterization of proteins by sedimentation equilibrium in the analytical ultracentrifuge, Chap. 14, 1st edn. New York, NY, U.S.A.: Academic Press, Inc.
35. Kumosinski TF, Pessen H. Methods in enzymology (117) part J: Enzyme structure. In: Hirs CHW, Timasheff SN, Eds. (1985) Structural interpretation of hydrodynamic measurements of proteins in solution through correlations with X-ray data, Chap. 11. New York, NY, U.S.A.: Academic Press, Inc.
36. Brown PH, Balbo A, Schuck P (2008) Characterizing protein–protein interactions by sedimentation velocity analytical ultracentrifugation. Curr Protoc Immunol Vol. 81 18:Unit 18.15, pp. 1–39.
37. Durchschlag H. Specific volumes of biological macromolecules and some other molecules of biological interest. In: (1986) Thermodynamic data for biochemistry and biotechnology. Hinz, H-J ed. Berlin, Heidelberg: Springer, pp. 45–128.
38. Gokarn Y, Agarwal S, Arthur K, Bepperling A, Day ES, Filoti D, Greene DG, Hayes D, Kroe-Barrett R, Laue T, Lin J, McGarry B, Razinkov V, Singh S, Taing R, Vankataramani S, Weiss WIII, Yang D, Zarraga IE (2015) Biophysical techniques for characterizing the higher order structure and interactions of monoclonal antibodies. ACS Symp Ser 1201:285–327.

39. Gokarn YR, Fesinmeyer RM, Saluja A, Razinkov V, Chase SF, Laue TM, Brems DN (2011) Effective charge measurements reveal selective and preferential accumulation of anions, but not cations, at the protein surface in dilute salt solutions. Protein Sci 20:580–587.
40. Vidarsson G, Dekkers G, Rispens T (2014) IgG subclasses and allotypes: from structure to effector functions. Front Immunol 5:520.
41. Yang D, Kroe-Barrett R, Singh S, Roberts CJ, Laue TM (2017) IgG cooperativity—Is there allostery? Implications for antibody functions and therapeutic antibody development. mAbs 9:1231–1252.
42. Diebolder CA, Beurskens FJ, de Jong RN, Koning RI, Strumane K, Lindorfer MA, Voorhorst M, Ugurlar D, Rosati S, Heck AJR, van de Winkel JGJ, Wilson IA, Koster EJ, Taylor RP, Saphire EO, Burton DR, Schuurman J, Gros P, Parren PWHI (2014) Complement is activated by IgG hexamers assembled at the cell surface. Science 343:1260–1263.
43. Wright RT, Hayes DB, Stafford WF, Sherwood PJ, Correia JJ (2018) Characterization of therapeutic antibodies in the presence of human serum proteins by AU-FDS analytical ultracentrifugation. Anal Biochem, 550:72–83.